

# Condensation on Superhydrophobic Copper Oxide Nanostructures

by

Nicholas Dou

Submitted to the Department of Mechanical Engineering  
in partial fulfillment of the requirements for the degree of

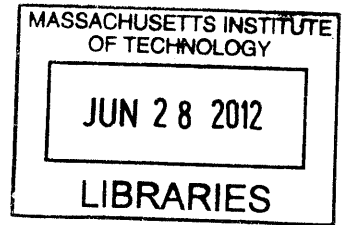
Bachelor of Science in Mechanical Engineering

at the

MASSACHUSETTS INSTITUTE OF TECHNOLOGY

June 2012

**ARCHIVES**



© Massachusetts Institute of Technology 2012. All rights reserved.

*N. Dou*

Author .....  
Department of Mechanical Engineering  
May 25, 2012

Certified by .....  
Evelyn N. Wang  
Associate Professor of Mechanical Engineering  
Thesis Supervisor

Accepted by .....  
John H. Lienhard V  
Samuel C. Collins Professor of Mechanical Engineering  
Undergraduate Officer



# Condensation on Superhydrophobic Copper Oxide Nanostructures

by

Nicholas Dou

Submitted to the Department of Mechanical Engineering  
on May 25, 2012, in partial fulfillment of the  
requirements for the degree of  
Bachelor of Science in Mechanical Engineering

## Abstract

Condensation is an important process in many power generation and water desalination technologies. Superhydrophobic nanostructured surfaces have unique condensation properties that may enhance heat transfer through a mechanism driven by surface tension. The increased droplet removal rate and reduced size of departing droplets facilitates improvements over traditional filmwise and dropwise condensation. This work investigates copper oxide nanostructures as a potential substrate for superhydrophobic condensation. We first explored and refined a procedure for creating and functionalizing oxide nanostructures on copper surfaces. The condensation behavior of these samples was characterized using an optical microscope and an environmental scanning electron microscope by quantifying the distribution of nucleation sites and droplet growth behavior. Using the knowledge gained from these studies, an experimental test bed was designed and fabricated to measure macro-scale condensation heat transfer for flat and tubular sample geometries. Preliminary results validate previous theoretical and experimental studies of filmwise condensation and demonstrate heat transfer enhancement with dropwise condensation. The copper oxide nanostructures exhibited jumping, which shows the effectiveness of the synthesis procedure.

Thesis Supervisor: Evelyn N. Wang

Title: Associate Professor of Mechanical Engineering



## Acknowledgments

I'd like to acknowledge my thesis advisor, Professor Evelyn Wang, for graciously giving me this research opportunity as well as valuable academic advice. I would also like to thank Dr. Ryan Enright for directly supervising my work and imparting invaluable theoretical and practical knowledge to me. Thanks to Dr. Youngsuk Nam and Nenad Miljkovic for working closely with me on this exciting project. Many thanks to the UROP program and MIT Energy Initiative for funding my summer research.



# Contents

<b>1</b>	<b>Introduction</b>	<b>11</b>
1.1	Dropwise condensation . . . . .	11
1.2	Superhydrophobic condensation . . . . .	12
1.2.1	Jumping . . . . .	14
1.3	Thesis overview . . . . .	14
<b>2</b>	<b>Surface synthesis and characterization</b>	<b>17</b>
2.1	Synthesis procedure . . . . .	17
2.2	Condensation characterization . . . . .	20
2.3	Results and discussion . . . . .	21
<b>3</b>	<b>Macro-scale condensation measurement</b>	<b>23</b>
3.1	Experimental design . . . . .	23
3.1.1	Vacuum chamber . . . . .	24
3.1.2	Condenser . . . . .	25
3.1.3	Coolant . . . . .	26
3.2	Heat transfer analysis . . . . .	27
3.3	Preliminary results and discussion . . . . .	29
<b>4</b>	<b>Conclusions</b>	<b>31</b>
4.1	Future Work . . . . .	31



# List of Figures

1-1	[Reproduced from Boreyko 2009 [1]] (a) Dropwise condensation on a smooth hydrophobic substrate and (b) on a rough superhydrophobic substrate where the micropillars are visible. Both substrates were horizontally oriented. Stages 1-3 of the condensation process characterize the initial nucleation, immobile coalescence, and mobile coalescence, respectively. (c) The surface coverage, which reached a plateau for both the hydrophobic and superhydrophobic surfaces but fluctuated because of the small field of view. Time 0 corresponds to the first visual appearance of condensate drops, and the error bars are the 95% confidence intervals of the exponential fit. . . . .	15
2-1	[Figure credit: Y. Nam] Scanning electron microscope (SEM) images of a sample during preparation show (a) the $\text{Cu}_2\text{O}$ intermediate layer after 1 minute and (b) the self-limited $\text{CuO}$ nanostructures after 5 minutes. (c) An X-ray diffraction pattern shows the composition of the surfaces after oxide integration. . . . .	18
2-2	Macroscopic Cassie state droplet placed on a gold/thiol functionalized surface with contact angle $\theta^{CB} = 169.7 \pm 2^\circ$ . . . . .	19
2-3	Copper oxide nanostructures (a) before and (b) after PDFA deposition (40 nm). . . . .	19
2-4	Diagram of the optical microscope setup used to observe condensation behavior. . . . .	20

2-5	(a) OM image showing nucleation site locations for a gold/thiol functionalized sample at a supersaturation of $S \approx 1.5$ . The image was captured at $t = 10$ s, prior to the onset of droplet coalescence. (b) Image processing yielded the coordinates of each site and (c) a script calculated the nearest neighbor distances, demonstrating agreement with a Poisson distribution and thus spatial randomness of nucleation sites. . . . .	21
3-1	Vacuum chamber (a) photo and (b) diagram with resistive heating elements that prevent unwanted condensation on chamber walls. This configuration is capable of outputting 2 kW when connected to a 120 V supply. . . . .	24
3-2	Condenser diagram. . . . .	25
3-3	Coolant flow diagram. . . . .	26
3-4	Initial images and heat flux results for (a) FWC on smooth copper, (b) DWC on silane functionalized copper, and (b) SHC on superhydrophobic copper oxide nanostructures. The consistency of data to Nusselt film theory for FCW demonstrates validity of the measurements. . . .	28

# Chapter 1

## Introduction

Many common industrial systems such as power plants, water desalinators, and heat pipes rely on condensation, a two-phase heat and mass transfer process that utilizes the working fluid's heat of vaporization. Latent heat transfer facilitates much larger heat flux than sensible heat transfer, which is important for these two-phase thermodynamic systems. Increasing heat transfer coefficients of condenser surfaces can provide further performance improvements without increasing physical size. One way to do this involves modifying condensation properties by engineering the chemistry and nano-scale structure of these surfaces.

### 1.1 Dropwise condensation

Currently, condensation can be classified into two main modes, filmwise and dropwise. Filmwise condensation (FWC), where a thin liquid film wets the condensing surface, is known to be the least desired mode due to the high thermal resistance of the condensate film. Dropwise condensation (DWC) occurs when the condensing surface is non-wetting, resulting in discrete droplets forming on the surface and shedding at millimetric length scales.

Although dropwise condensation is highly desired, most industrial systems use filmwise condensation. DWC can achieve heat fluxes that are an order of magnitude higher than that of FWC since it leaves areas of the condensing surface exposed to

vapor, which become low-resistance locations for droplets to nucleate [3]. Hydrophobic surfaces that exhibit DWC exist in nature – leaves, for example – but can also be synthesized with a nonpolar coating.

For DWC to be most effective, droplets must be quickly removed from the surface as the condensate accumulates, since the poor thermal conductance of large droplets inhibits heat transfer. Condensate removal typically depends on gravity. When the droplet reaches a certain critical mass, its weight overcomes surface adhesion forces and it rolls off of the surface. The dimensionless Bond number describes this force balance

$$Bo = \frac{\Delta\rho g R^2}{\gamma} \quad (1.1)$$

and the capillary length describes the characteristic length scale at which both forces are relevant

$$\lambda_c = \sqrt{\frac{\gamma}{\rho g}} \quad (1.2)$$

where  $\rho$  is density (or the density difference between liquid and vapor),  $g$  is gravitational acceleration,  $R$  is droplet size, and  $\gamma$  is surface tension [7]. The capillary length suggests an approximate droplet shedding size on the order of  $\lambda_c \sim 1$  mm. Previous experimentation has shown that water droplets larger than  $100 \mu\text{m}$  do not contribute significantly to heat transfer. Clearly, DWC would benefit from an additional droplet removal mechanism that acts on smaller droplets.

## 1.2 Superhydrophobic condensation

The unique interfacial properties of superhydrophobic nanostructured surfaces promote a special type of DWC known as superhydrophobic condensation (SHC) that offers potential improvements in heat transfer performance. On these types of surfaces, the contact angle of condensation droplets is very high such that they barely wet the surface. Due to roughness, two distinct wetting states exist: the Cassie-Baxter state, in which a droplet is suspended (or mostly suspended) on top of air-filled nanostructures, and the Wenzel state, in which a droplet wets the inner cavities of

the nanostructures. SHC requires stable growth of Cassie state droplets [6].

To ensure formation and persistence of Cassie droplets, an energy criterion must be met. During droplet growth, the pinning energy barrier that prevents contact line advancement at the base of the nanostructures is given by

$$\cos \theta_a^W = r \cos \theta_a \quad (1.3)$$

where  $\theta_a$  is the advancing contact angle and  $r$  is the roughness factor of the surface. Roughness is defined as the ratio of the total surface area to the apparent projected area. The spreading energy barrier required to advance the droplet over the tops of the nanostructures is given by

$$\cos \theta_a^{CB} = -1 \quad (1.4)$$

The ratio of these energies determines droplet morphology during condensation by delineating two regimes.

$$E^* = \frac{\cos \theta_a^{CB}}{\cos \theta_a^W} = \frac{-1}{r \cos \theta_a} \quad (1.5)$$

When  $E^* > 1$  the base contact line advances with each droplet and the Wenzel state dominates. In contrast, when  $E^* < 1$  the contact line is pinned as each droplet spreads over the discontinuous surface above the nanostructures and the Cassie state dominates. Thus,  $E^*$  must be less than 1 [5].

A second criterion for Cassie-stable SHC requires that the the mean separation between droplet nucleation sites  $\langle L \rangle$  be at least twice as large as the characteristic roughness size that defines the pinning energy barrier  $l$ .

$$\frac{\langle L \rangle}{l} \gtrsim 2 \quad (1.6)$$

This ensures that droplets have enough space to spread before they meet a neighboring droplet [5].

### 1.2.1 Jumping

The strict conditions of SHC give rise to an interesting surface phenomenon known as “jumping.” A jumping event occurs when two neighboring Cassie-state droplets coalesce. The reduced curvature of the combined droplet causes a small amount of surface energy release. Since the droplets are weakly pinned to the substrate, a large fraction of this energy gets converted into out-of-plane kinetic energy that launches the merged droplet away from the surface. Essentially, this becomes another droplet removal mechanism that reduces the characteristic droplet shedding size to  $R \sim 10 \mu\text{m}$ , which is much smaller than the capillary length [1].

A recent study defined three stages of SHC: initial droplet growth without coalescence, immobile coalescence, and mobile coalescence [1]. DWC encompasses only the first two stages, the second of which includes the merging of droplets without an appreciable change in center of mass before and after the event. Self-propelled removal during the third stage of SHC results in a plateau in average droplet diameter, as illustrated visually in Fig. 1-1. In addition, the surface coverage stabilizes at a significantly lower value for SHC than DWC, which indicates clear potential for heat transfer improvement.

## 1.3 Thesis overview

My thesis project investigates copper oxide nanostructures as a substrate for superhydrophobic condensation. We first developed of a scalable synthesis procedure that is compatible with existing heat transfer materials and industrial-scale processes. This was tested on flat and tubular samples, which were examined with optical microscopy and environmental scanning electron microscopy to characterize the condensation behavior, specifically the distribution of nucleation sites and droplet growth behavior. We then designed and constructed a vacuum chamber setup to measure macro-scale heat transfer across flat and tubular samples in the absence of non-condensable gases. Preliminary measurements from this setup are presented.

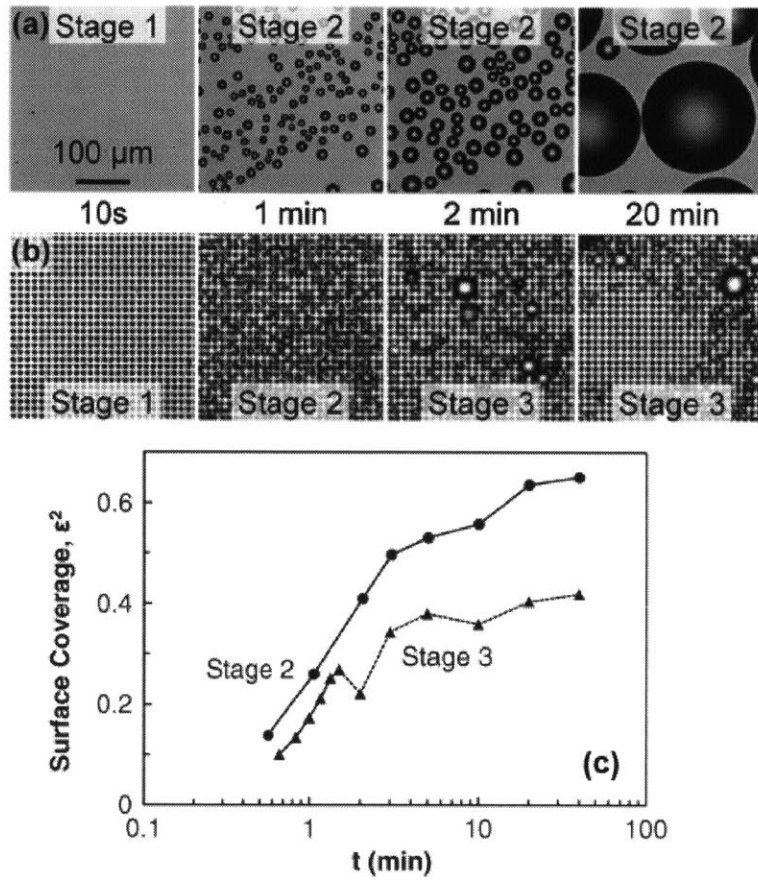


Figure 1-1: [Reproduced from Boreyko 2009 [1]] (a) Dropwise condensation on a smooth hydrophobic substrate and (b) on a rough superhydrophobic substrate where the micropillars are visible. Both substrates were horizontally oriented. Stages 1-3 of the condensation process characterize the initial nucleation, immobile coalescence, and mobile coalescence, respectively. (c) The surface coverage, which reached a plateau for both the hydrophobic and superhydrophobic surfaces but fluctuated because of the small field of view. Time 0 corresponds to the first visual appearance of condensate drops, and the error bars are the 95% confidence intervals of the exponential fit.



# Chapter 2

## Surface synthesis and characterization

The process of creating superhydrophobic copper oxide nanostructures involves cleaning the substrate, integrating oxide nanostructures, and functionalizing the surface to induce hydrophobicity. Once samples were synthesized, SHC was verified and characterized under a microscope.

### 2.1 Synthesis procedure

Commercially available copper sheets (0.8 mm thickness) cut into  $2 \times 2$  cm tabs and 1/4" tubing (0.25" OD, 0.186" ID) cut into 6.25" lengths are used as substrates for the test samples. Each sample is first cleaned in an ultrasonic bath with acetone for approximately 5 mins and then rinsed with ethanol, IPA, and deionized (DI) water to remove organic contaminants. Native oxide is etched away by immersing samples into a 2.0 M hydrochloric acid solution, rinsing with DI water, and drying with nitrogen.

Copper oxide nanostructures are integrated onto each cleaned surface by immersion in a heated ( $\sim 95$  °C) alkaline solution composed of  $\text{NaClO}_2$ ,  $\text{NaOH}$ ,  $\text{Na}_3\text{PO}_4 \cdot 12 \text{H}_2\text{O}$  (3.75 : 5 : 10 wt%). The chemical reaction that produces the oxide structures occurs in two steps. A thin  $\text{Cu}_2\text{O}$  layer ( $< 200$  nm) is initially created on the substrate,

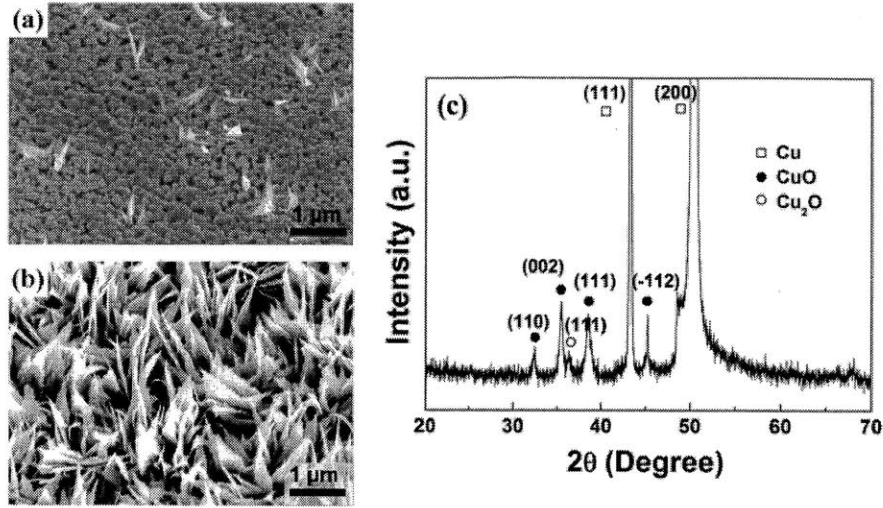
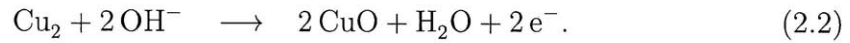
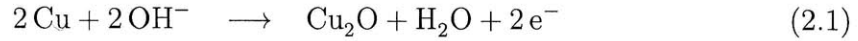


Figure 2-1: [Figure credit: Y. Nam] Scanning electron microscope (SEM) images of a sample during preparation show (a) the  $\text{Cu}_2\text{O}$  intermediate layer after 1 minute and (b) the self-limited  $\text{CuO}$  nanostructures after 5 minutes. (c) An X-ray diffraction pattern shows the composition of the surfaces after oxide integration.

which is oxidized again to create  $\text{CuO}$  [2]. Specifically, the chemical reactions are



In 5 minutes, the oxide nanostructures grow to a height of  $1\ \mu\text{m}$ , after which the growth rate slows significantly. The oxide layer passivates the copper substrate at this point, preventing further growth of the oxide features [5]. This self-limiting behavior helps to minimize the parasitic thermal resistance of the nanostructures, since oxide has poor conductivity. An X-ray diffraction pattern shown in Fig. 2-1 reveals the chemical composition of the samples, with strong  $\text{CuO}$  peaks and weaker  $\text{Cu}_2\text{O}$  peaks from the intermediate layer underneath. Contact angle measurements using water and formamide were used to obtain the effective solid fraction  $\varphi_{eff} = 0.027 \pm 0.011$  and the effective roughness  $r_{eff} = 10.2 \pm 2.8$ .

After integration of nanostructures, the samples must be functionalized. A few procedures were attempted to achieve this goal. One stable surface chemistry is a self-assembled monolayer of 1H,1H,2H,2H-perfluorodecanethiol deposited on an initial

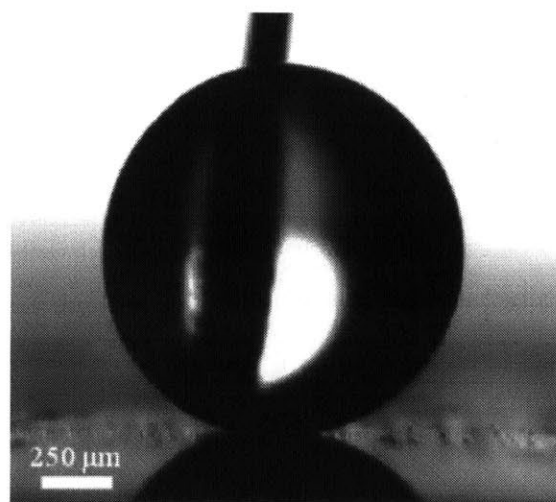


Figure 2-2: Macroscopic Cassie state droplet placed on a gold/thiol functionalized surface with contact angle  $\theta^{CB} = 169.7 \pm 2^\circ$

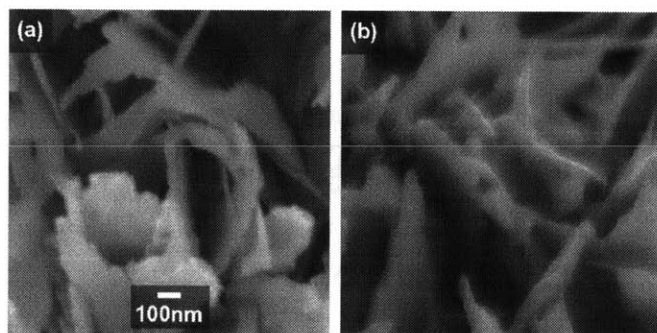


Figure 2-3: Copper oxide nanostructures (a) before and (b) after PDFA deposition (40 nm).

30 nm coating of gold. This is done by immersion in a 1 mM ethanol solution for 1 hour. Goniometer measurements reveal an equilibrium angle of  $\theta_e = 113.5^\circ \pm 3^\circ$  for these samples.

PFDA and silane are also effective in functionalizing the oxide surfaces. For these chemicals, the samples are placed in a desiccator with a small quantity of liquid while vacuum is applied to the chamber. The liquid evaporates and bonds to the samples by chemical vapor deposition (CVD). PFDA creates a 40 nm layer on the nanostructures that was observed using SEM imagery in Fig. 2-3.

## 2.2 Condensation characterization

Droplet nucleation and growth is observed under an optical microscope using the experimental setup depicted in Fig. 2-4. Dry nitrogen is bubbled through a heated water reservoir to create a source of saturated air. Adjusting the water reservoir temperature directly controls the supersaturation of the air  $S = p_v/p_w$ . A three-way valve enables rapid switching between the saturated air and dry air from a bypass line. This valve delivers air to a plastic enclosure under the microscope, which rests on top of a temperature-controlled cold stage. At the beginning of each experiment, the sample is attached to the stage with thermal grease to ensure good conduction and then dried with nitrogen. When the stage temperature equilibrates to the test temperature  $T_w = 283 \pm 0.1$  K, the valve is toggled to initiate flow of saturated air to the sample enclosure at a constant rate of  $Q = 2.5$  L/min, indicating the start of the experiment. During the experiment, a high-speed CMOS camera captures the condensation process through a  $40\times$  or  $100\times$  microscope objective and a probe inside the enclosure tracks humidity.  $800 \times 600$  images are recorded every 0.1 seconds.

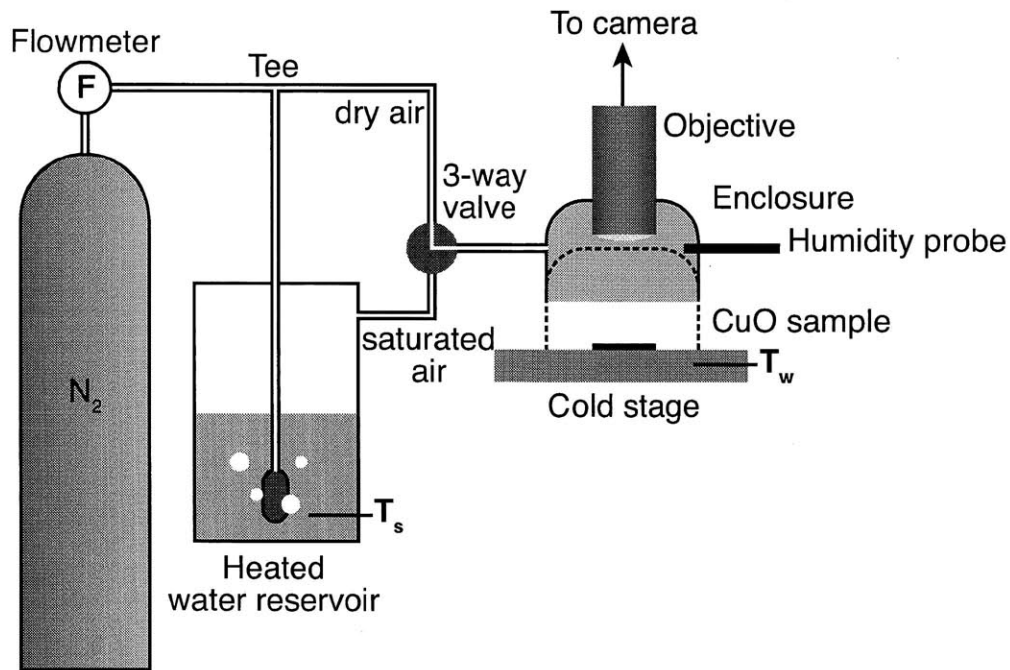


Figure 2-4: Diagram of the optical microscope setup used to observe condensation behavior.

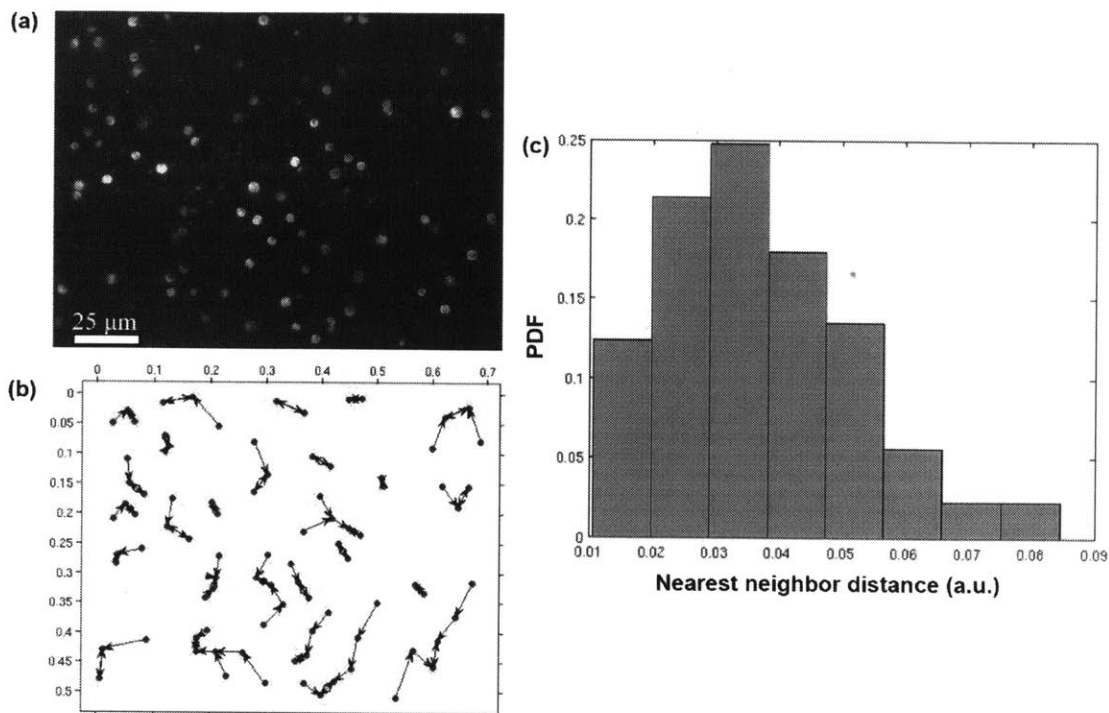


Figure 2-5: (a) OM image showing nucleation site locations for a gold/thiol functionalized sample at a supersaturation of  $S \approx 1.5$ . The image was captured at  $t = 10$  s, prior to the onset of droplet coalescence. (b) Image processing yielded the coordinates of each site and (c) a script calculated the nearest neighbor distances, demonstrating agreement with a Poisson distribution and thus spatial randomness of nucleation sites.

## 2.3 Results and discussion

Observations from the optical microscope setup helped to determine the distribution of nucleation sites. Specifically, an image taken prior to the onset of droplet coalescence was analyzed, assuming that a single droplet formed at each nucleation site. Using ImageJ and Photoshop to pinpoint each droplet and MATLAB to find the nearest neighbor distances resulted in the nucleation site distribution shown in Fig. 2-5. The outcome is consistent with a Poisson distribution, indicating that the sites were spatially random.

Growth behavior of condensate on the CuO nanostructures was examined under an environmental scanning electron microscope (ESEM). Qualitatively, droplets exhibited Cassie state characteristics, which is consistent with the estimated pinning

energy ratio,  $E^* \approx 0.19$ . To analyze the effect of coalescence, the droplet size distribution and density were measured from several images. Since the mean center-to-center distance between droplets was  $\sim 5 \mu\text{m}$  (inferred from droplet density), the fact that most droplets were smaller than  $10 \mu\text{m}$  suggests that jumping played a significant role in condensate removal. Therefore the samples were clearly experiencing SHC.

# Chapter 3

## Macro-scale condensation measurement

A macro-scale condensation setup was designed to measure the heat transfer performance of SHC on copper oxide nanostructures. This setup consists of a condenser contained within an environmental chamber, which can create high temperatures and heat fluxes to simulate real world industrial systems. The chamber can also sustain a vacuum to eliminate noncondensable gases. This chapter documents the construction of the experimental setup along with some initial results.

### 3.1 Experimental design

At the most basic level, a condenser converts vapor into liquid by cooling it, thus transferring heat from the vapor to the coolant. The apparatus for this experiment must create highly controlled conditions for condensation to occur on a test surface and take measurements during the process so that heat transfer can be calculated. All of the equipment and instrumentation in the condensation setup work together to accomplish these goals.

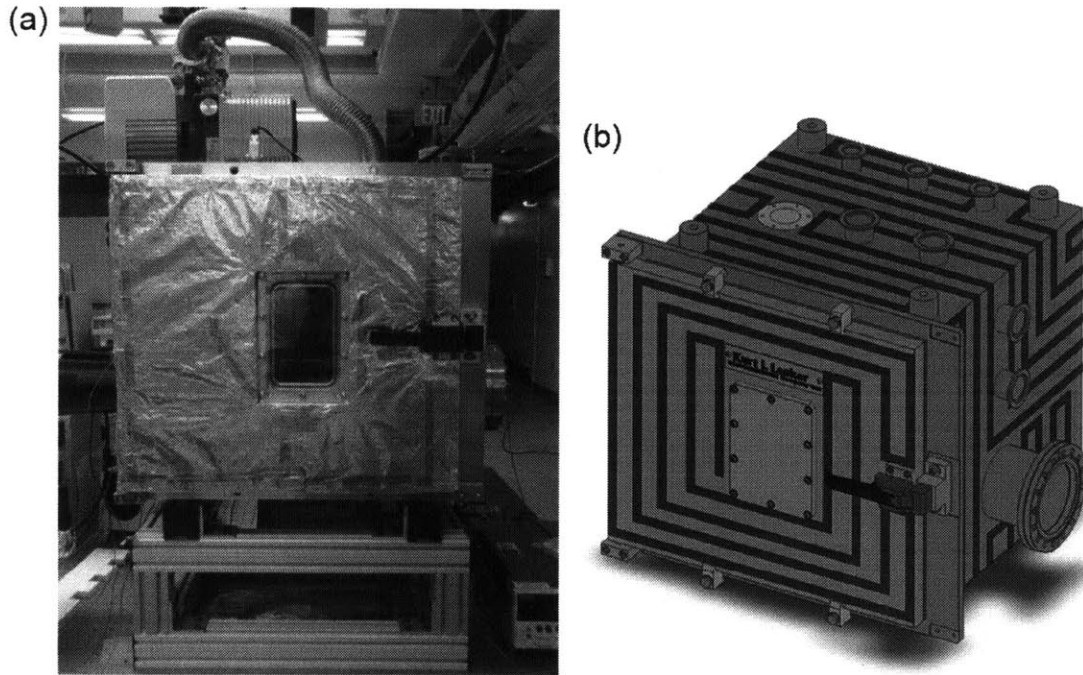


Figure 3-1: Vacuum chamber (a) photo and (b) diagram with resistive heating elements that prevent unwanted condensation on chamber walls. This configuration is capable of outputting 2kW when connected to a 120 V supply.

### 3.1.1 Vacuum chamber

Before starting the experiment, a pump evacuates a cubic steel vacuum chamber (side length  $\sim 0.5$  m), reducing the internal pressure from atmospheric levels down to  $P_{min} < 1$  Pa. A liquid-nitrogen-cooled cold trap condenses all excess vapor from the vacuum line to ensure complete dryness inside the chamber. After degassing the chamber, a needle valve is opened to introduce water vapor from a heated reservoir, creating a saturated environment. To prevent condensation on chamber walls, the entire chamber is heated using resistive elements and wrapped in insulation. Fig. 3-1 depicts the intricate layout of the heating elements used to ensure sufficient and uniform heating. Three elements connected in parallel are capable of delivering 2 kW of power to the chamber when connected to a 120 V supply. This operating point is designed to maintain the chamber at a temperature of  $80^\circ\text{C}$  during a condensation experiment.

Pulling a vacuum in the chamber is important in order to control the gas com-

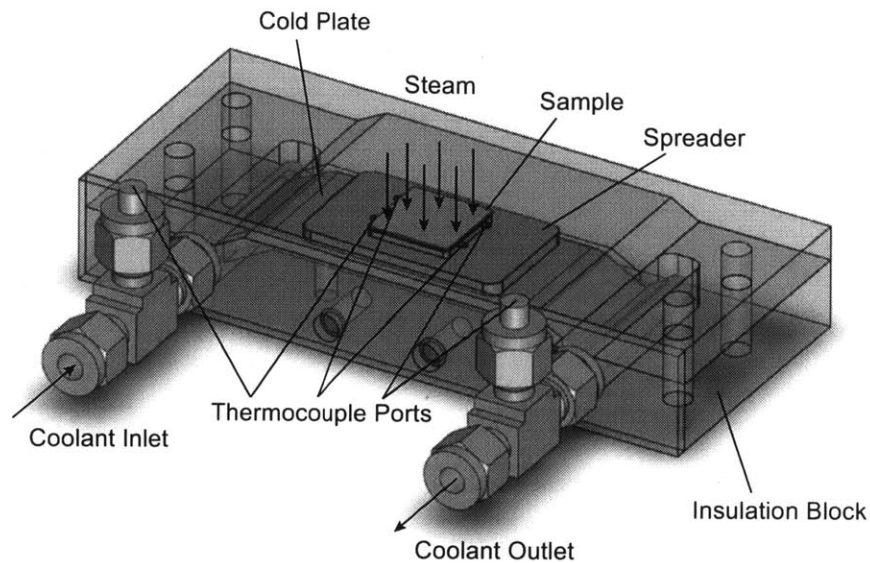


Figure 3-2: Condenser diagram.

position of the environment. In particular, noncondensable gases (NCG) can impede the condensation process. The conversion of vapor into liquid results in a significant volume and pressure drop due to the density difference between the two phases. This pressure gradient causes transport of NCG to the vicinity of the condensing surface. NCG do not condense under these conditions and their presence creates a mass diffusion resistance for water vapor to reach the heat transfer surface. Thus, removing them from the chamber is desirable.

### 3.1.2 Condenser

To test flat surfaces, a condenser block was built. As illustrated in Fig. 3-2, this block consists of a copper flat-tube cold plate (thermal resistance of  $0.33\text{ }^{\circ}\text{C cm}^2/\text{W}$  at 1 GPM) encapsulated by insulating plastic. The Ultem insulation block is designed to minimize heat loss and was custom machined to fit the cold plate. A copper spreader that is soldered to the cold plate provides a  $2 \times 2$  cm mounting surface for the sample. To ensure good thermal contact, a separate sample holder clamps the surface in place. The cold plate itself is driven by chilled water that passes through inlet and outlet ports. Two thermocouple ports monitor inlet and outlet temperatures, and

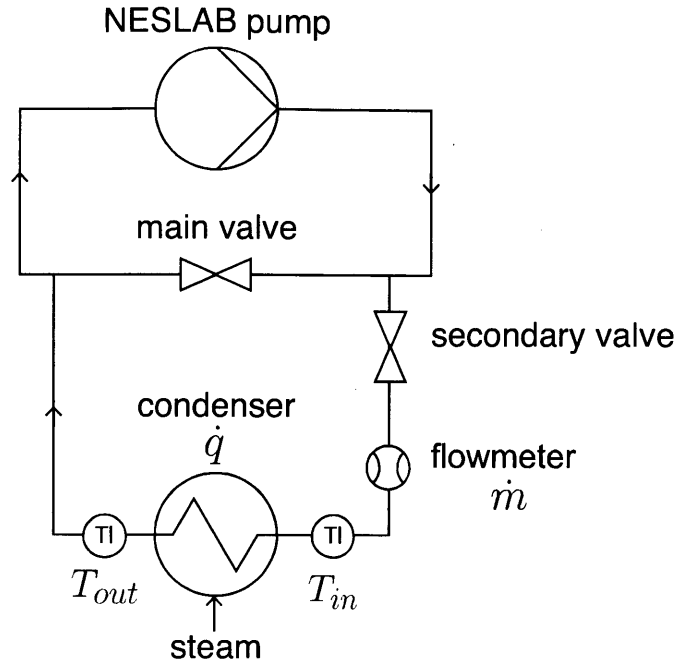


Figure 3-3: Coolant flow diagram.

four thermocouple channels monitor wall temperature on the backside of the sample.

The modularity of the system makes it easy to test tubular surfaces as well. This is done by simply removing the condenser block and connecting the coolant lines directly to the sample. Thermocouples at the inlet and outlet provide sufficient information for heat transfer calculation in this configuration.

### 3.1.3 Coolant

The working fluid used to cool the sample comes from a chilled water main. Fig. 3-3 shows the high level design of the coolant lines. Essentially, the NESLAB pump drives water through a main loop composed of 1" diameter plastic tubing. The secondary loop steps the tube diameter down to 1/2" and then 1/4" before entering the vacuum chamber where the condenser resides. Foam insulation along the entire line mitigates heat loss. A main valve and secondary valve offer coarse and fine control of flow rate, which is measured by a very precise flowmeter. An experiment is initiated by turning on these valves.

## 3.2 Heat transfer analysis

Heat transfer rate can be calculated during an experiment using the known flow rate and the temperature drop across the condenser. Specifically, the heat flux is

$$q'' = \frac{\dot{m}c_p}{A}(T_{out} - T_{in}). \quad (3.1)$$

where  $\dot{m}$  is the mass flow rate,  $c_p$  is the specific heat of the coolant,  $A$  is the area of the condenser, and the temperatures are measured at the condenser inlet and outlet [7]. This heat is dissipated between the coolant and the vapor inside the chamber.

For the case of tubular samples, the thermal pathway for heat transfer includes convection between the coolant and the inner wall of the sample, conduction through the copper wall, and finally the condensation resistance between the outer wall and water vapor. The total resistance of this series pathway is just the sum of all resistances

$$\frac{\Delta T}{\dot{Q}} = R_{tot} = R_{coolant} + R_{Cu} + R_{condensation} = \frac{1}{h_i A_i} + \frac{r_o - r_i}{k_{Cu} A_m} + \frac{1}{h_o A_o} \quad (3.2)$$

where  $k$  is thermal conductivity and  $h$  is the heat transfer coefficient [8].  $h$  is directly related to the dimensionless Nusselt number

$$Nu = \frac{hL}{k} \quad (3.3)$$

which is the ratio of convective to conductive heat transfer across a boundary. Empirical correlations relating the Nusselt number to physical fluid and solid characteristics exist for a wide variety of geometries. The resistance can be used to predict heat flux based on a given temperature difference, or to deduce the heat transfer coefficient of condensation.

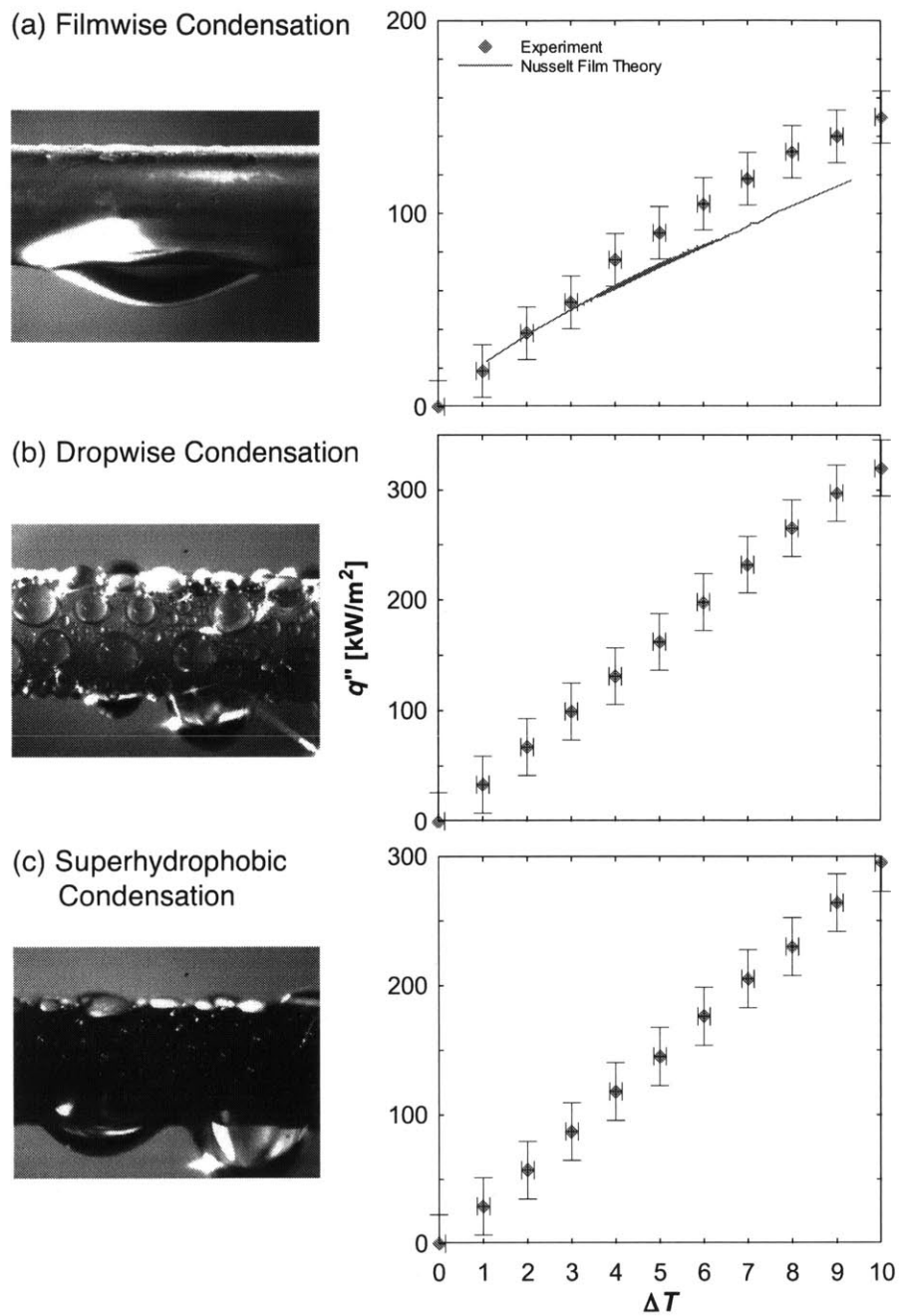


Figure 3-4: Initial images and heat flux results for (a) FWC on smooth copper, (b) DWC on silane functionalized copper, and (b) SHC on superhydrophobic copper oxide nanostructures. The consistency of data to Nusselt film theory for FCW demonstrates validity of the measurements.

### 3.3 Preliminary results and discussion

Preliminary experiments were done on tubular samples to measure heat flux for FWC on smooth copper, DWC on functionalized copper, and SHC on superhydrophobic copper oxide nanostructures. Fig. 3-4 shows these results. Nusselt film theory was used to calculate the total resistance of the heat transfer pathway for FCW and predict the heat flux based on the temperature difference across the condenser ports. The experimental results match the theoretical model well, thus validating the accuracy of the experimental setup.

SHC did not show significant improvement in heat transfer performance over DWC in these initial tests. A look at the condensation image reveals similarity in droplet sizes and relatively low contact angles for SHC. By observation, these large Wenzel droplets are pinned to the surface and do not exhibit jumping behavior when they merge with other droplets. The large thermal resistance of these droplets prevents effective heat transfer. Defects or degradation of the silane coating could have caused this.



# Chapter 4

## Conclusions

The phenomenon of jumping that occurs during superhydrophobic condensation provides a mechanism for droplet removal at length scales much smaller than the capillary length. This indicates a potential for heat transfer improvement in industrial condensers by modifying surface chemistry and structure.

A scalable procedure for synthesizing superhydrophobic copper oxide nanostructures was developed and characterized. These structures are able to sustain stable Cassie growth and droplet jumping, which are characteristic of superhydrophobic condensation. Several different functionalization methods were tested to induce hydrophobicity.

In order to test the macro-scale heat transfer performance of these surfaces, a condensation chamber was constructed. This chamber was designed to sustain high temperatures and heat fluxes in an environment free of noncondensable gases. Initial experiments validate system accuracy with results in accordance with filmwise condensation theory and demonstrate the increased heat transfer performance of dropwise condensation.

### 4.1 Future Work

Robustness is one of the primary challenges of implementing engineered surfaces in industrial thermodynamic systems. Droplet pinning observed during preliminary tests

showed evidence of coating inconsistency or instability. Additional investigation is required to elucidate the cause of this and to discover the most reliable functionalization chemistry. Furthermore, the reliability of nanostructures themselves should be examined. To refine structure properties, immersion duration and chemical composition of the oxidation solution can be adjusted.

Improvement of the synthesis process should be done in parallel with heat transfer measurement. Using the condensation rig, the benefits of superhydrophobic condensation can be quantified. Since most real-world systems contain noncondensable gases, it would be informative to study their effect on heat transfer. The vacuum chamber facilitates control of gas content.

The development of a synthesis procedure for superhydrophobic copper oxide nanostructures and a condensation experimental setup are important steps towards creating high performance condensers. Incorporation of these enhanced devices in industrial systems can improve the efficiency of power generation and water desalination, an important goal in light of today's energy crisis.

# Bibliography

- [1] J.B. Boreyko and C.-H. Chen. Self-propelled dropwise condensate on superhydrophobic surfaces. *Physical Review Letters*, 108(18), 2009.
- [2] G.M. Brisard. Application of probe beam deflection to study the electrooxidation of copper in alkaline media. *Electrochimica Acta*, 40(7):859–865, 1995.
- [3] B. Chung, M.C. Kim, and M. Ahmadinejad. Filmwise and dropwise condensation of steam on short inclined plates. *Journal of Mechanical Science and Technology*, 22, 2008.
- [4] R. Enright. Superhydrophobic condensation: The role of energy barriers and size-scale. 2011.
- [5] R. Enright, N. Dou, N. Miljkovic, Y. Nam, and E.N. Wang. Condensation on superhydrophobic copper oxide nanostructures. In *Proceedings of the 3rd Micro/Nanoscale Heat and Mass Transfer International Conference*, March 2012.
- [6] D. Quéré. Wetting and roughness. *Annual Review of Materials Research*, 38(1):71–99, 2008.
- [7] W. M. Rohsenow, J.P.Hartnett, and E.N.Ganid. *Handbook of heat transfer fundamentals*. McGraw-Hill, Inc, 1985.
- [8] E.H. Young and D.E. Briggs. The condensing of low pressure steam on vertical rows of horizontal copper and titanium tubes. *A.I.Ch.E Journal*, 12(1), 1965.